Temporal dynamics of binocular integration in primary visual cortex

Michele A. Cox Department of Psychology, College of Arts and Science, Vanderbilt Vision Research Center, Center for Cognitive and Integrative Neuroscience, Vanderbilt University, Nashville, TN, USA

Kacie Dougherty Department of Psychology, College of Arts and Science, Vanderbilt Vision Research Center, Center for Cognitive and Integrative Neuroscience, Vanderbilt University, Nashville, TN, USA

Jacob A. Westerberg Department of Psychology, College of Arts and Science, Vanderbilt Vision Research Center, Center for Cognitive and Integrative Neuroscience, Vanderbilt University, Nashville, TN, USA

Michelle S. Schall Department of Psychology, College of Arts and Science, Vanderbilt Vision Research Center, Center for Cognitive and Integrative Neuroscience, Vanderbilt University, Nashville, TN, USA

Alexander Maier Department of Psychology, College of Arts and Science, Vanderbilt Vision Research Center, Center for Cognitive and Integrative Neuroscience, Vanderbilt University, Nashville, TN, USA

Whenever we open our eyes, our brain quickly integrates the two eyes' perspectives into a combined view. This process of binocular integration happens so rapidly that even incompatible stimuli are briefly fused before one eye's view is suppressed in favor of the other (binocular rivalry). The neuronal basis for this brief period of fusion during incompatible binocular stimulation is unclear. Neuroanatomically, the eyes provide two largely separate streams of information that are integrated into a binocular response by the primary visual cortex (V1). However, the temporal dynamics underlying the formation of this binocular response are largely unknown. To address this question, we examined the temporal profile of binocular responses in V1 of fixating monkeys. We found that V1 processes binocular stimuli in a dynamic sequence that comprises at least two distinct temporal phases. An initial transient phase is characterized by enhanced spiking responses for both compatible and incompatible binocular stimuli compared to monocular stimulation. This transient is followed by a sustained response that differed markedly between congruent and incongruent binocular stimulation. Specifically, incompatible binocular stimulation resulted in overall response reduction relative to monocular stimulation (binocular suppression). In contrast, responses to compatible stimuli were either suppressed or enhanced (binocular facilitation) depending on the neurons' ocularity (selectivity for one eye over the other) and laminar location. These results suggest that binocular integration in V1 occurs in at least two sequential steps that comprise initial additive combination of the two eyes' signals followed by widespread differentiation between binocular concordance and discordance.

Introduction

The primate binocular visual field is the largest among mammals (Heesy, 2004). Ocular convergence

Citation: Cox, M. A., Dougherty, K., Westerberg, J. A., Schall, M. S., & Maier, A. (2019). Temporal dynamics of binocular integration in primary visual cortex. *Journal of Vision*, *19*(12):13, 1–21, https://doi.org/10.1167/19.12.13.

https://doi.org/10.1167/19.12.13 Received July 3, 2018; published October 17, 2019 ISSN 1534-7362 Copyright 2019 The Authors

This work is licensed under a Creative Commons Attribution-NonCommercial-NoDerivatives 4.0 International License.

Downloaded from abstracts.iovs.org on 04/26/2024

comes at the cost of total visual-field size but improves visual perception in several ways: Stereopsis allows for fine depth discrimination and binocular fusion can compensate for the retinal blind spot as well as certain kinds of visual occlusion (Howard, 2012; Howard & Rogers, 2012). Furthermore, binocular viewing increases visual acuity and contrast sensitivity compared to viewing with one eye alone (Blake & Fox, 1973; Jones & Lee, 1981). These perceptual benefits of binocular vision require that inputs from the two eyes be rapidly integrated and combined into a singular coherent (cyclopean) view by the visual system. However, the two eyes' views are almost never identical and often differ substantially (Wheatstone, 1838). Thus, the visual system must contain fast-acting mechanisms for both detecting binocular concordance and resolving interocular differences (Tanabe & Cumming, 2014).

The brain prioritizes rapid fusion of the two eyes' views to the extent that even incongruent binocular stimuli are briefly fused before one eye's image dominates (i.e., binocular rivalry). Specifically, when grating stimuli of orthogonal orientation are presented briefly (~150 ms), observers report a fused percept that resembles a plaid (Carter & Cavanagh, 2007; Katyal, He, & Engel, 2015; Wolfe, 1983). Following this brief period of fusion, binocular rivalry ensues, and observers perceive one of the two gratings at a time (Blake & Logothetis, 2002). Previous work has shown that alternating perceptual states during binocular rivalry correlate with changes in cortical activity (Gail, Brinksmeyer, & Eckhorn, 2004; Keliris, Logothetis, & Tolias, 2010; Knapen, Brascamp, Pearson, van Ee, & Blake, 2011; Lee, Blake, & Heeger, 2005; Leopold & Logothetis, 1996; Macknik & Martinez-Conde, 2004; Maier, Logothetis, & Leopold, 2007; Maier, Wilke, Aura, Zhu, Ye, & Leopold, 2008; Panagiotaropoulos, Deco, Kapoor, & Logothetis, 2012; Polonsky, Blake, Braun, & Heeger, 2000; Schmid & Maier, 2015; Sheinberg & Logothetis, 1997; Sterzer & Rees, 2008; Tong & Engel, 2001; Tong, Nakayama, Vaughan, & Kanwisher, 1998; Wilke, Logothetis, & Leopold, 2006). Yet little is known about the temporal dynamics of cortical responses directly following the onset of binocular rivalry—or, indeed, binocular stimulation in general.

Anatomically, the retinogeniculate projections and the geniculocortical projections are largely segregated by eye until they converge onto single neurons within primary visual cortex (V1; Casagrande & Boyd, 1996; Dougherty, Schmid, & Maier, 2018). Geniculate axons from each eye terminate in horizontally alternating bands within V1's granular layer (layer 4C in old-world primates), giving rise to tangential regions of neurons that share eye preference, known as *ocular dominance columns* (Hendrickson, Wilson, & Ogren, 1978; Hubel & Freeman, 1977). The functional consequence of this organization is that most V1 neurons respond more vigorously to stimulation in one eye compared to the other, though only a small minority of V1 neurons respond to one eye exclusively (Hubel & Wiesel, 1968; Kato, Bishop, & Orban, 1981; Malach, Amir, Harel, & Grinvald, 1993; Smith et al., 1997). V1 neurons also exhibit tangentially organized selectivity for other stimulus features such as spatial frequency and orientation (Hubel & Wiesel, 1968; Ringach, Hawken, & Shapley, 1997; Nauhaus, Nielsen, & Callaway, 2016; Nauhaus, Nielsen, Disney, & Callaway, 2012). Given that its neurons encode both detailed stimulus features and eye-of-origin information, V1 is thought to play a critical role in detecting and resolving interocular differences (for reviews, see Blake & Wilson, 2011; Cumming & DeAngelis, 2001; Tong, Meng, & Blake, 2006).

Since most V1 neurons receive inputs from both eyes, one might expect their synaptic activation to increase when both eyes are stimulated compared to stimulation of one eye alone, a phenomenon termed *interocular facilitation* or *binocular facilitation* (Figure 1). Yet several studies have reported decreases in spiking activity during binocular stimulation compared to monocular stimulation (Endo, Kaas, Jain, Smith, & Chino, 2000; Kumagami, Zhang, Smith, & Chino, 2000), a phenomenon termed *interocular suppression* or *binocular suppression* (Bishop, Burke, & Davis, 1959; Vastola, 1960). A particularly well-studied variant of binocular suppression is dichoptic cross-orientation suppression (dCOS). During dCOS, a neuron's response to an optimally oriented stimulus viewed by the neuron's preferred eye is reduced by the presentation of an orthogonally oriented stimulus in the other eye (Sengpiel, Baddeley, Freeman, Harrad, & Blakemore, 1998; Sengpiel & Blakemore, 1994; Sengpiel, Blakemore, & Harrad, 1995; Sengpiel, Freeman, & Blakemore, 1995; Sengpiel & Vorobyov, 2005). This type of visual stimulation instigates the perceptual phenomenon of binocular rivalry, where each eye's view randomly alternates in perceptual dominance (Blake & Logothetis, 2002). However, by definition dCOS does not fluctuate with perceptual state. Instead, it resembles a more generally depressed state of cortical visual processing that affects many V1 neurons simultaneously, independently of which eye they favor (Sengpiel, Blakemore, & Harrad, 1995).

Several authors have theorized that the cortical suppression during dCOS enables or initiates binocular rivalry (Sengpiel, Blakemore, & Harrad, 1995). A strong indicator that dCOS would be involved in the initiation of binocular rivalry is if it slightly precedes or coincides with the ~150-ms delayed onset of binocular rivalry. Yet we know little about the temporal dynamics of dCOS. Indeed, we know little about the

Downloaded from abstracts.iovs.org on 04/20/2024

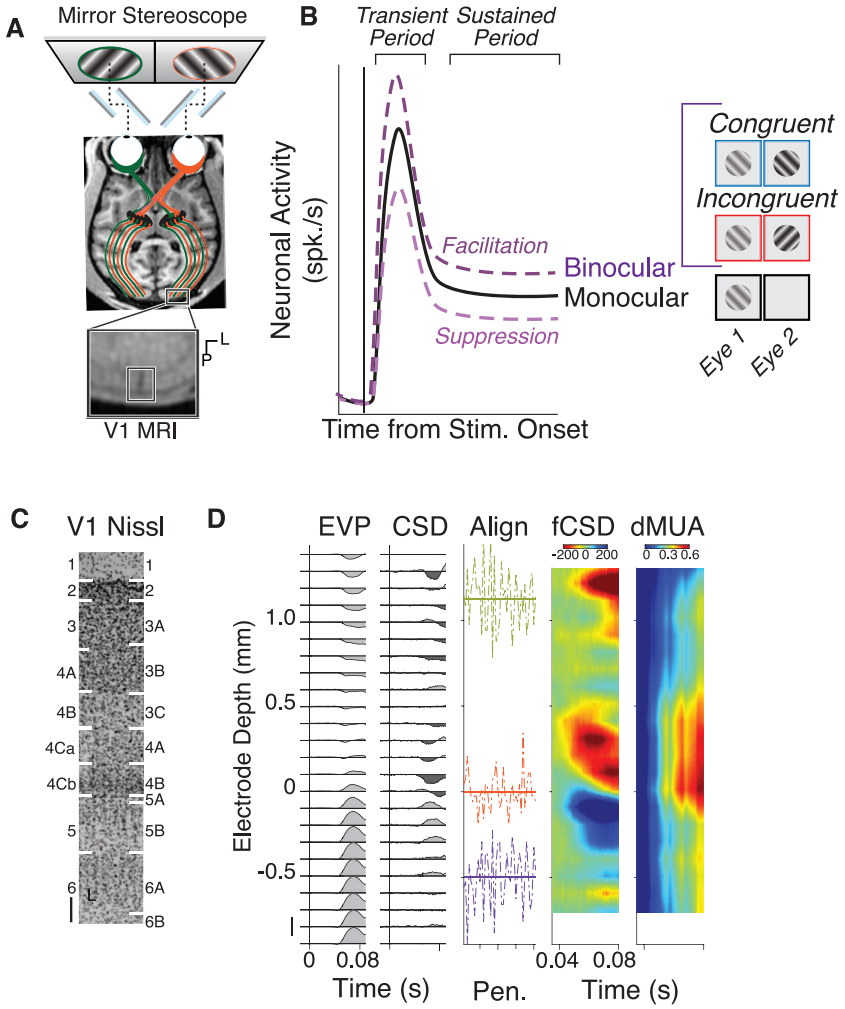

Figure 1. (A) This study uses stereoscopic visual stimulation in awake, behaving monkeys combined with simultaneous recordings of single-neuron responses across the laminar microcircuit of primary visual cortex (V1) to determine the temporal dynamics of binocular integration in V1. Monkeys sat in front of a mirror stereoscope that provided independent visual stimulation of either eye (top). The signals from each retina are largely segregated until they converge onto single neurons within V1. The pathway from each retina is represented using orange and green traces overlaid on an axial MRI scan (middle). Electrode penetrations targeting the perifoveal region of V1 produced cerebrospinal fluid tracks that we traced via anatomical MRI (bottom, white box; Monkey 1). (B) Our main aim was to examine the temporal profile of V1 responses to stimulating one or both eyes. Stimuli could appear in the neurons' preferred (dominant) eye only (monocular) or both eyes (binocular). In the binocular condition, stimuli were either of the same orientation (congruent) or of orthogonal orientation (incongruent). There are three possible outcomes for how binocular stimulation modulates V1 spiking: no difference from monocular stimulation, increased activity (facilitation; upper dashed purple line), or decreased activity (suppression; lower dashed purple line). (C) Nissl-stained section of V1 labeled according to Brodmann's (left) and Hassler's (right) schemes. Note the distinct concentration of neurons in the middle layers (Brodmann's 4Ca/b and Hassler's 4A/B), which coincides with the bulk of inputs from the lateral geniculate nucleus to V1. (D) Neurophysiological criteria used to determine laminar alignment. EVP: Evoked visual potential computed by averaging the local field potential response to a brief (88 ms) black-to-white flash of the display monitor ($n = 271$ trials; scale bar represents ± 63 μV and ± 0.1 mm). CSD: Current source density response computed from EVP (scale bar represents ± 474 nA/mm^3). Negative deflections (black) indicate current sinks and positive deflections (gray) indicate current sources. Align: Functionally determined depth of the top of V1 (green), the bottom of V1's middle granular input (orange), and the bottom of V1 (purple) across all penetrations (abscissa) examined for this study ($n = 41$; see Table 1). Ordinate is in relative units. On average, the bottom of the granular Layer 4 was located 1.2 mm from the top of V1 and 0.5 mm from the bottom of V1. fCSD: Flash-evoked CSD, averaged across penetrations and interpolated in the vertical dimension (10 points per 0.1 mm^3). dMUA: Flash-evoked multiunit response, normalized to the maximum response and then averaged across penetrations.

Downloaded from abstracts.iovs.org on 04/20/2024

temporal dynamics of binocular integration more generally, because the majority of previous studies have averaged stimulus responses over time.

Here we combined stereoscopic visual stimulation in awake, behaving monkeys with simultaneous recordings of single-neuron responses across the V1 laminar microcircuit to determine the temporal dynamics of binocular integration and dCOS in V1. The temporal evolution of binocular signals across the V1 microcircuit is particularly informative regarding the sequence of computational processes underlying integration of the two eyes' signals, given V1's laminar organization: The bulk of retinal activation initially impacts V1's middle, granular layers before progressing to the upper, supragranular (Layers 2/3) and deep, infragranular layers (Layers 5/6; Callaway, 1998; Douglas & Martin, 2004). We observed a universal, transient increase in spiking activity, roughly 150 ms in duration, whenever both eyes were stimulated compared to one eye alone. Following this initial period of additive binocular combination, V1 neurons sustained either binocular facilitation or binocular suppression, depending on their ocularity and laminar position.

Methods

Subjects

Two adult monkeys (*Macaca radiata*, one female) were used in this study. All procedures adhered to the Association for Research in Vision and Ophthalmology Animal Statement, followed regulations by the Association for the Assessment and Accreditation of Laboratory Animal Care, were approved by Vanderbilt University's Institutional Animal Care and Use Committee, and observed National Institutes of Health guidelines.

Surgical procedures

In a series of surgeries, each monkey was implanted with a custom-designed MRI-compatible plastic head holder and a plastic recording chamber (Schmiedt et al., 2014). All surgeries were performed under sterile surgical conditions using isoflurane anesthesia (1.5%–2.0%). Vital signs, including blood pressure, heart rate, SpO_2, CO_2, respiratory rate, and body temperature, were monitored continuously. During surgery, the head holder and a recording chamber were attached to the skull using transcranial ceramic screws (Thomas Recording, Gießen, Germany) and self-curing denture acrylic (Lang Dental Manufacturing, Wheeling, IL). A craniotomy was performed over the perifoveal visual-field representation of primary visual cortex (both hemispheres in each monkey) concurrent with the position of the recording chamber. Each monkey was given analgesics and antibiotics for postsurgical care.

Visual stimulation

Stimuli were presented on CRT monitors running at either 60 Hz (resolution 1,280 × 1,024 pixels; $N = 7$ sessions) or 85 Hz (resolution 1,024 × 768; $N = 23$ sessions). CRT monitors were linearized by measuring the luminance of the monitor at 17 brightness increments, linearly spaced between the minimum and maximum for each gun (red, green, and blue), using either a photometer or a spectroradiometer (PhotoResearch, Syracuse, NY). We fitted the measured luminance changes to a power function and then applied the inverse of the exponent of this power function for each R, G, and B value during stimulus generation. Visual stimuli were generated by MonkeyLogic (Asaad & Eskandar, 2008; Asaad, Santhanam, McClellan, & Freedman, 2013) for MATLAB (R2012-2014; MathWorks, Natick, MA) running on a PC (Dell, Round Rock, TX; Windows 7 or 10) with an Nvidia graphics card. MonkeyLogic also synchronized behavioral events and gaze position. Gaze position was measured using infrared light-sensitive cameras, which visualized the eye through infrared-transparent mirrors (Qian & Brascamp, 2017), and commercially available eye-tracking software (EyeLink II or SMI Research), which was converted to an analog signal that was sampled by MonkeyLogic/MATLAB (NIDAQ PCI-6229) at 1 kHz.

Animals viewed all stimuli through a custom-built mirror stereoscope (Carmel, Arcaro, Kastner, & Hasson, 2010), such that images on the right side of the forward-positioned display were viewed by the right eye and images on the left by the left eye (Figure 1A; the monitor was divided by a black, nonreflective septum). The total viewing distance from each eye to the monitor ranged between 46 and 57 cm, resulting in 20.5 to 34.5 pixels/° of visual angle (°va). To facilitate fusion, an oval aperture was displayed at the edge of each half-screen. At the beginning of each experimental session, the stereoscope was calibrated via a behavioral task (Maier et al., 2008), which required the animals to fixate on the same location in visual space while being cued in one eye only. Gaze position was measured for each fixation location and compared across eyes. When gaze position was comparable for cueing in each eye, the mirrors were considered aligned.

Behavioral tasks

Both monkeys were trained to hold their gaze on a small (0.2°va) spot presented in the center of the

Downloaded from abstracts.iovs.org on 04/20/2024

monitor for extended periods of time (2–3 s) while circular gratings or other stimuli were presented in the perifoveal visual field. If gaze remained fixed within 1°va of the fixation cue for the duration of the trial, the monkey received a juice reward. No other responses were required. These parameters apply to the receptive-field, tuning, and dichoptic paradigms described later.

Neurophysiological apparatus

Extracellular voltage fluctuations were recorded using acute linear multielectrode arrays (UProbe, Plexon Inc., Dallas, TX; Vector Arrays, NeuroNexus, Ann Arbor, MI) inside an electromagnetic radio frequency-shielded booth. The number of microelectrode contacts varied between probes (UProbe = 24, Vector Arrays = 32), but contacts were always linearly spaced 0.1 mm apart. Voltage fluctuating signals were amplified, filtered, and digitized using a 128-channel Cerebus neural signal processing system (Blackrock Microsystems, Salt Lake City, UT). Two signals were recorded and stored for subsequent off-line analysis: a broadband (0.3 Hz–7.5 kHz) signal sampled at 30 kHz and a low-pass filtered signal (0.3–500 Hz) sampled at 1 kHz. The low-pass filtered signal was used as a measure of the local field potential (LFP). Spiking activity was extracted from the 30-kHz broadband signal as described later.

The neural signal processing system also recorded nonneurophysiological analog signals related to the monitor refresh (i.e., a photodiode signal; OSI Optoelectronics, Montreal, Quebec) and eye position (i.e., voltage output of eye-tracking system), which were digitized and stored at 30 and 1 kHz, respectively. It stored time-stamped event markers sent from the behavioral control system (MonkeyLogic). These time stamps and the photodiode signal were used to align the time-varying intracranial data with the occurrence of key visual and behavioral events.

Neurophysiological signals

With the exception of LFPs, all neurophysiological signals were extracted off-line from the recorded broadband signal using custom-written code in MATLAB (version 2016a). We computed two measures of multiunit activity: an *analog* signal (aMUA) and a *discretized* signal (dMUA). The analog signal was computed by high-pass filtering the broadband signal at 750 Hz with a fourth-order Butterworth filter and rectifying (Supèr & Roelfsema, 2005). The discretized signal was computed by applying a time-varying threshold to the envelope of the broadband signal, with an impulse recorded at every time point where the signal envelope exceeded the threshold. This procedure is analogous to the initial step of spike sorting without an ensuing step of cluster analysis. For both the threshold and envelope computations, we began by low-pass filtering the 30-kHz-sampled voltage signals at 5 kHz with a second-order Butterworth filter. We then downsampled the signal by a factor of 3, high-pass filtered at 1 kHz using a second-order Butterworth filter, and then rectified the resulting data. For the envelope computation, we further downsampled the signal by a factor of 3. For the threshold computation, we smoothed the signal by convolving the data with a 1-s boxcar function and then multiplied the result by 2.2. To recover temporal information, we extracted ±0.3 ms of data from the original signal for each time point where the envelope exceeded the threshold. We then adjusted the time point to correspond with the point of maximum slope within this window—that is, aligning to the spike waveform. For all MUA signals, a multiunit describes the neuronal signal extracted using the techniques described here from a single microelectrode contact from a single penetration.

We also extracted single-unit activity (SUA) via Kilosort, an unsupervised machine-learning spike-sorting algorithm (Pachitariu, Steinmetz, Kadir, Carandini, & Harris, 2016). A major benefit of using Kilosort for extracting single-unit activity from linear electrode arrays is that neurons that produce a signal on more than one microelectrode contact are not counted more than once. We used the default parameters for sorting and cluster merging, so we focus here on our customized postprocessing steps only. For all clusters detected by Kilosort, we extracted ±1 ms of data around each spike from the original broadband signal for each simultaneously recorded electrode contact. We averaged across all extracted impulses to create a spatiotemporal map of the spike waveform (time × electrode contacts). To be included in the study, the region of the spatiotemporal waveform map that exceeded ±30% of maximum modulus had to span less than 0.9 ms and three neighboring microelectrode contact (0.3 mm). Clusters that met these criteria were localized to the microelectrode contact with the largest amplitude.

Spike rates for each dMUA and SUA were limited to 1 kHz (except dMUA in Figure 1D). In all cases, spiking data were convolved using a Poisson distribution resembling a postsynaptic potential (Hanes, Thompson, & Schall, 1995), with the spike rate R computed at time t:

$$R(t) = \left[1 - \exp\left(-\frac{t}{\tau_g}\right)\right] * \left[\exp\left(-\frac{t}{\tau_d}\right)\right],$$

where τ_g and τ_d are the time constants for growth and decay, respectively. Data from previous studies suggest values of 1 and 20 for τ_g and τ_d, respectively (Sayer,

Downloaded from abstracts.iovs.org on 04/20/2024

Friedlander, & Redman, 1990). For aMUA, this kernel was convolved with the filtered and rectified time-varying signal directly. For dMUA and SUA, impulse times were converted to a time-varying signal using 0 to represent time points without an impulse and 1 for time points where an impulse was detected, and then convolved. After convolution, the signal was multiplied by the sampling frequency to convert to spikes per second.

Current source density (CSD) analysis was performed on the LFP signal using an estimate of the second spatial derivative appropriate for multiple contact points (Nicholson & Freeman, 1975):

$$\mathrm{CSD}(t,\, c) = -\frac{x(t, c-z) + x(t, c+z) - 2x(t,\, c)}{z^2},$$

where x is the extracellular voltage recorded in volts at time t from an electrode contact at position c, and z is the electrode intercontact distance (0.1 mm). In order to yield CSD in units of current per unit volume, the resulting CSD from the formula was multiplied by 0.4 S/mm as an estimate of cortical conductivity (Logothetis, Kayser, & Oeltermann, 2007).

Receptive-field paradigm and analysis

Monkeys fixated a central cue while circular patches of static random noise were displayed at pseudorandomized locations within a predetermined virtual grid (Figure 2A). Noise patches were generated by multiplying a 2-D Gaussian with a randomized patch of full-contrast black and white pixels and then cropping at radius = 3*σ. Noise-patch size, grid extent, and grid spacing were manually determined by the experimenter each session. The receptive-field mapping procedure typically started with a coarse mapping phase that covered a whole visual quadrant (θ = 0°–90°, eccentricity = 0°va–8°va) using relatively large stimuli (σ = 1°va–2°va) and grid spacing (i.e., 2°va–5°va). This coarse mapping then was followed by a finer mapping phase (σ = 0.125°va–0.5°va, spacing = 0.25°va–1°va) focused on the portion of the visual field that contained the receptive fields of the neurons under study. Up to five stimuli were shown per trial, for 200 ms each with 200-ms blank periods interleaved. We used retinotopic 3-D receptive-field matrices (RFMs; Cox et al., 2013) to compute spatial maps of neuronal responses as a function of visual space (Figure 2B and 2C). For each stimulus presentation, the response of a given unit (i.e., MUA from a single microelectrode contact or SUA) was averaged to produce a single scalar value (0.05–0.25 s from stimulus onset). These scalar values were converted to units of z score (n = all stimulus presentations, regardless of stimulus parameters). Then, for each trial, the retinotopic portion of the RFM corresponding to the noise-patch location (radius = σ) was filled with that value. This procedure produced a matrix consisting of one dimension for vertical visual space, one for horizontal visual space, and one for stimulus presentations. This third dimension was then collapsed via averaging, producing a spatial map of each unit's response. Receptive-field centers and extents were computed by fitting an oval to the largest contiguous patch of the spatial map that exceeded 1 z score (e.g., black line in top of Figure 2B).

Tuning paradigm and analysis

Monkeys fixated a central cue while circular grating patches appeared at a single location in parafoveal visual space, determined by the results of the receptive-field paradigm and analysis. Up to five stimuli were shown per trial, typically for 250 ms each with 250-ms blank periods interleaved. Each sinusoidal grating patch could vary in eye, orientation, spatial frequency, and phase (Figure 2D). Binocular stimulation always consisted of identical stimuli in both eyes (dioptic presentations). Parameters were determined by the experimenter each session based on assessment of audible multiunit responses to the stimuli described here, and typically included some combination of monocular and dioptic stimuli varying in orientation by at least five steps between 0° and 180°. Contrast was held steady at a Michelson contrast of 0.9 or 1.0. Stimulus-evoked responses were averaged 0.05–0.25 s from stimulus onset for each trial. In computation of orientation tuning curves as well as determination of ocularity (Figure 2E), all nonrelevant parameters were matched (e.g., for comparison between responses evoked by each eye, orientation and phase were balanced between the eyes). Preferred orientation was typically consistent across neurons collected on different V1-residing multielectrode contacts in a single penetration of the linear array (see Intersession alignment; a detailed description of the laminar distribution of orientation tuning is the focus of upcoming work). The preferred orientations that were established online (see Determining orientation tuning and ocular bias) determined the stimulus orientations used in the dichoptic paradigm.

Dichoptic paradigm and analysis

Monkeys fixated on a central cue while circular grating patches appeared at a single location in parafoveal visual space, determined by the results of the receptive-field paradigm and analysis. Up to three stimuli were shown per trial, typically for 500 ms each with 500-ms blank periods interleaved. Sinusoidal

Downloaded from abstracts.iovs.org on 04/20/2024

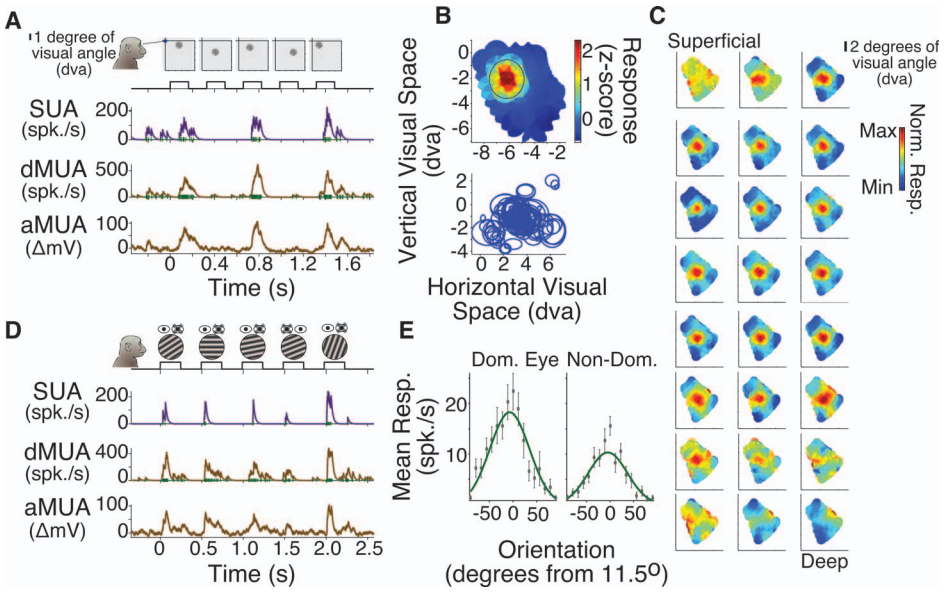

Figure 2. (A) Receptive-field mapping using static random noise patches. Single-trial responses of each single unit and multiunit activity (SUA, dMUA, and aMUA) to the stimuli pictured. For SUA and dMUA, green vertical lines indicate a detected spike. Purple and tan lines are the result of convolving individual spikes with an EPSP-shaped kernel. For aMUA, the tan line is the result of convolving the rectified, high-passed extracellular voltage signal using the same kernel. (B) Top: Example SUA receptive-field matrix showing neuronal responses as a function of visual space. *Z*-axis is in units of *z* score, computed across all stimulus presentations ($n = 658$). Black circle signifies the receptive-field boundary. Bottom: Receptive-field boundaries for all SUA ($n = 152$) as a function of visual space. (C) Receptive-field matrices extracted from the dMUA signal at each microelectrode contact in an example linear array penetration. Top left panel is the most superficial microelectrode contact, bottom right panel is the deepest. Conventions for each receptive-field matrix plot are as in (B), though the *z*-axis is scaled individually for each microelectrode contact. (D) Determining orientation selectivity using grating patches (tuning paradigm); all conventions as in (A). (E) SUA as a function of grating orientation for presentations to the contralateral (left) and ipsilateral (right) eye. Error bars show standard error of the mean. Green lines are Gaussian fits.

grating patches varied between two orientations—determined by the results of the tuning paradigm and analysis—and contrasts, with spatial frequency and phase held constant. Stimuli were shown to each eye in isolation (monocular) and to both eyes simultaneously such that in some presentations the same orientation was shown to both eyes (binocular congruent) and on other trials the orientation differed between the eyes (binocular incongruent). Following the conventions used in previous studies (Sengpiel et al., 1998), the contrast in the dominant eye was approximately half of that in the nondominant eye (0.45 and 0.9 Michelson contrast for 18 penetrations and 70% of neurons, 0.5 and 1.0 for four penetrations and 12% of neurons, 0.4 and 1.0 for five penetrations and 18% of neurons). As the central aim of the study was to examine the effects of nondominant-eye stimulation on neuronal responses to dominant-eye stimulation with a preferred stimulus (Figure 1B), all stimulus conditions were defined relative to each neuron's preferred monocular condition. On the majority of penetrations ($N = 22$ of 30), this design was fully balanced. However, a few penetrations contained only the binocular congruent or binocular incongruent condition (Table 1). Note that for clarity we show only the neurons that were collected in both binocular conditions in some plots (i.e., Figures 3B through 3G, 4E through 4J, 6A through 6I, 7A through 7I), but as most statistical analyses (described later) compared responses for the binocular conditions to those for the monocular condition, we included all neurons in these analyses (reported in Results text or Table 2).

To analyze evoked responses, we calculated the mean response difference between the binocular and monocular conditions (ΔM) and performed a paired-sample, two-tailed t test. For both calculations, the monocular condition serves as the subtrahend, such that positive values for the mean difference and t statistic represent a greater response for the binocular condition (i.e., facilitation) and negative values represent a greater response for the monocular condition (i.e., suppression). We also computed a normalized binocular modulation index by taking the difference of the monocular and binocular responses, divided by their sum. This produced an index value ranging from −1 to 1. Here too, as the monocular condition always served as the numerator's subtrahend, positive binocular modulation index values indicate binocular facil-

Downloaded from abstracts.iovs.org on 04/20/2024

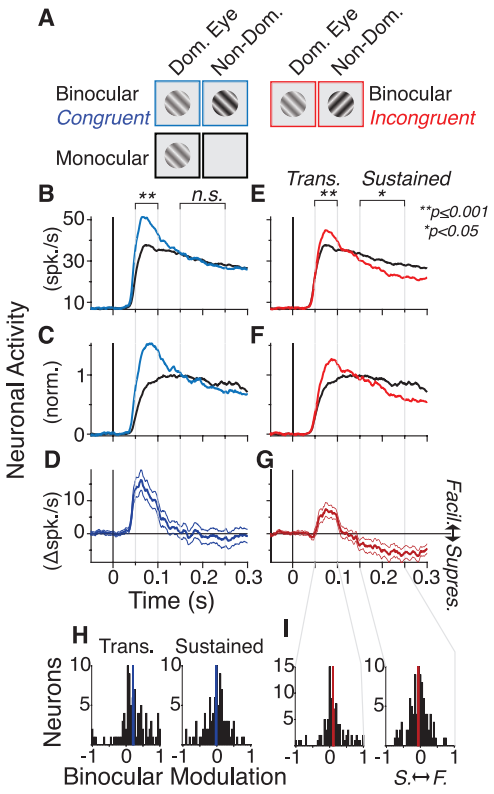

Figure 3. (A) Main stimulus conditions for the dichoptic paradigm: monocular (black), binocular congruent (blue), and binocular incongruent (red). We will use the same color convention to mark these stimulus conditions throughout this and all subsequent plots. Note that the contrast of the stimulus in the nondominant eye was approximately double that of the stimulus in the dominant eye (see Methods). (B) Mean V1 single-unit activity (SUA; ordinate) response to the binocular congruent stimulus (blue) compared to monocular stimulus presentation (black) as a function of time (0 = stimulus onset) across all units selective to either stimulus orientation, eye, or both features ($n = 80$) and sampled in both binocular conditions. Asterisks indicate significance from a paired-sample t test (binocular vs. monocular) over the indicated response phase (transient: 50–100 ms; sustained: 150–250 ms). (C) Same as (B), except SUA activity is normalized to the monocular condition before averaging across units. (D) Differential between the binocular congruent SUA response and the monocular SUA response. Subtraction was performed on a unit-by-unit level and then averaged across the populations (thin line = standard error of the mean). Positive values indicate binocular facilitation and negative values indicate binocular suppression. (E–G) Same as (B–D), but for the binocular incongruent condition (red line; $n = 80$). (H) Distribution of binocular modulation index of the congruent stimuli for the transient (left, 50–100 ms) and sustained (right, 150–250 ms) response phases ($n = 91$). Blue lines indicate the sample means (0.21 and −0.02, respectively). (I) Same as (H), but for the incongruent binocular stimuli ($n = 95$). Red lines indicate the sample means (0.11 and −0.03, respectively).

itation and negative values indicate binocular suppression. Finally, as we were particularly interested in the temporal dynamics of responses, all statistical analyses were performed after averaging over 50–100 ms ("transient" or "early" phase) or 150–250 ms ("sustained" or "late" phase) relative to stimulus onset.

Determining orientation tuning and ocular bias

Orientation tuning was determined by analyzing monocular and dioptic data from the tuning and dichoptic tasks and testing for a significant main effect of orientation via an analysis of variance. All other stimulus parameters (orientation, phase, contrast, spatial frequency, monocular vs. dioptic) were either balanced or included as groups in the analysis. Reponses were averaged over a time period ranging 50–250 ms from stimulus onset. Ocularity of each neuron was determined similarly. For a neuron to be included in this study it had to exhibit either a significant main effect of orientation with a response peak for one of the stimulus orientations used in the dichoptic task or a significant difference in response between the eyes when all other stimulus parameters were balanced (see Table 1). Neurons included in this study were further subdivided into three groups based on their ocularity and orientation tuning (i.e., Figure 4E through 4J; see also Table 1): Those that exhibited orientation tuning and but no significant difference in response between the eyes were considered tuned and *equiocular* (note that what we term equiocular is often referred to as "binocular" in the literature, but we avoid this term to distinguish between the neuronal response and stimulus conditions). Those that exhibited orientation tuning and a significant difference in response between the eyes were considered tuned and *ocular-biased*. Those that did not exhibit orientation tuning but exhibited a significant response difference between the eyes were considered untuned and ocular-biased.

Intersession alignment

The relative depth of each microelectrode contact in cortex was determined using several neurophysiological criteria (Figure 1D): The upper and lower bounds of V1 were determined algorithmically using data from the receptive-field and tuning paradigms. First, we used the magnitude of the stimulus-evoked dMUA response to a grating stimulus placed over the receptive field to determine which microelectrode contacts gave a reliable stimulus-evoked response (paired-sample t test between the mean response for the time periods −50 to 0 ms from stimulus onset and 50 to 100 ms following stimulus onset, family-wise error rate = 0.05; using all

Downloaded from abstracts.iovs.org on 04/20/2024

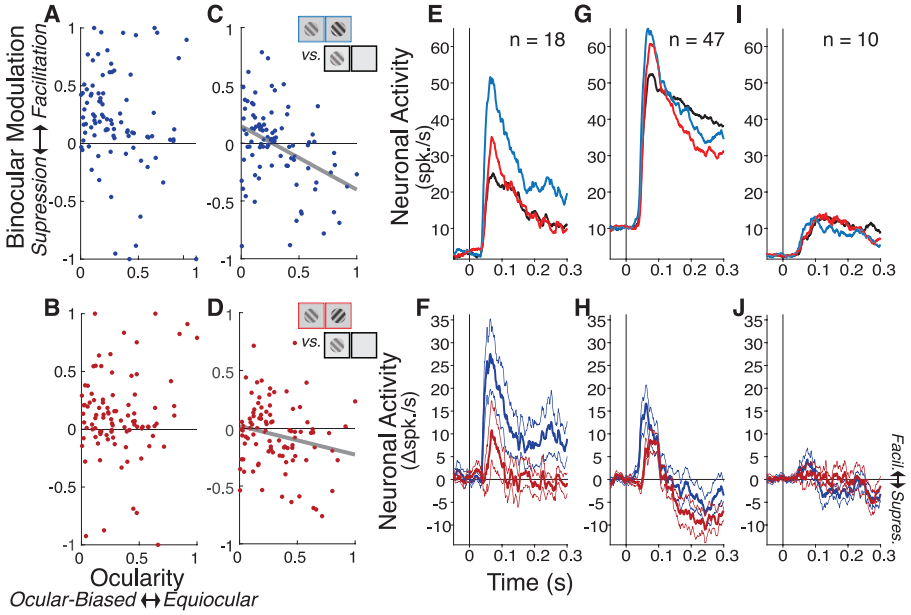

Figure 4. (A) Congruent binocular modulation during the transient phase as a function of each unit's ocularity ($n = 91$); no significant correlation. (B) Incongruent binocular modulation during the transient phase as a function of each neuron's ocularity ($n = 95$); no significant correlation. (C) Congruent binocular modulation during the sustained phase as a function of each neuron's ocularity ($n = 91$). Binocular modulation was significantly correlated with ocularity. (D) Incongruent binocular modulation during the sustained phase as a function of each neuron's ocularity ($n = 95$). Binocular modulation was significantly correlated with ocularity. (E) Mean single-unit activity response (ordinate) for the monocular (black), binocular congruent (blue), and binocular incongruent (red) conditions as a function of time (abscissa; 0 indicates stimulus onset) across all orientation-tuned equiocular neurons. Conventions as in Figure 3B. (F) Same data as in (E), plotted as a difference relative to monocular stimulation. Conventions as in Figure 3D. (G) Same as (E) but for orientation-tuned ocular-biased neurons. (H) Same data as in (G), plotted as a difference in response relative to monocular stimulation. (I) Same as (E) but for ocular-biased neurons that were not tuned to orientation. (J) Same data as in (I), plotted as a difference in response relative to monocular stimulation.

stimulus presentations regardless of stimulus parameters). We also extracted receptive fields from dMUA as described under Receptive-field paradigm and analysis. As dMUA does not rely on single-neuron isolation, we were able to compute RFMs for each microelectrode contact (Figure 2C) and use the criterion of 1 z score to determine the location and extent of each receptive field. An aggregate receptive-field center for each cortical location was calculated by averaging all concurrently measured receptive fields across depth. Then we checked that all dMUA-derived RFMs had a center within 0.25°va of the aggregate receptive-field center. In this way, receptive-field mapping information was used to identify spatial bounds of V1. Typically, this RFM-based analysis eliminated superficial and deep microelectrode contacts due to either not reaching the criterion of 1 z score within the RFM or a deviation of the receptive-field center (possibly due to penetrating another fold of cortex). In cases where the V1 bounds extracted from the evoked response differed from those extracted from the RFMs, we averaged the two sets of measures, rounding inward.

We used a well-established and histologically verified neurophysiological method to functionally determine

Binocular condition	Total penetrations	Total single units	Orientation and/or eye selective	Orientation and eye selective (tuned and ocular-biased)	Orientation selective only (tuned and equiocular)	Eye selective only (untuned and ocular-biased)
Congruent	24	115	91	50	23	18
Incongruent	29	135	95	56	18	21
Congruent or incongruent	30	152	106	59	23	24
Congruent and incongruent	22	98	80	47	18	15

Table 1. Number of single units isolated across 30 total penetrations (six in Monkey 2), for each population (columns) and binocular stimulus condition (rows). See Methods for details on single-unit extraction and classification.

Downloaded from abstracts.iovs.org on 04/20/2024

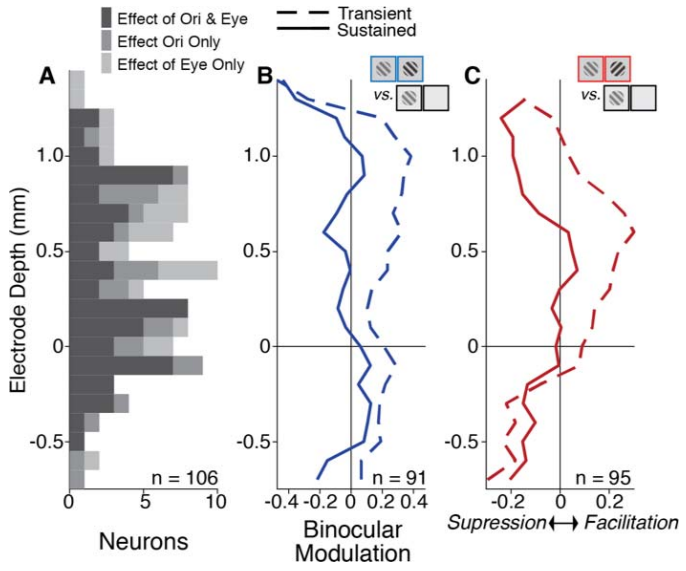

Figure 5. (A) Distribution of neurons across cortical depth, relative to Layer 4/5 boundary (ordinate = 0; see Methods). (B) Congruent binocular modulation (abscissa) as a function of cortical depth (ordinate) for the transient (dashed line) and sustained (solid line) response phases. The mean at each cortical depth includes neurons collected at the indicated depth as well as neurons located ±0.1 mm away (i.e., a sliding window average across depths) to account for low *n*. (C) Incongruent binocular modulation (abscissa) as a function of cortical depth (ordinate) for the transient (dashed line) and sustained (solid line) response phases. Conventions as in (B).

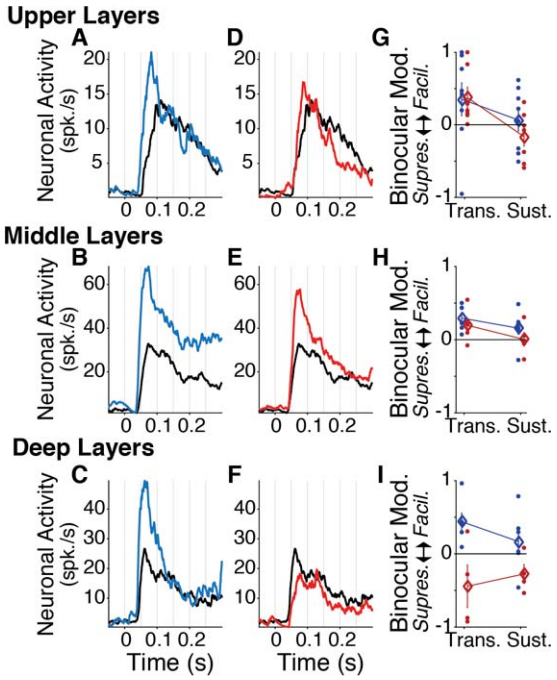

Figure 6. (A–C) Mean single-unit activity response to the binocular congruent (blue) and monocular (black) conditions across all tuned equiocular neurons as a function of laminar compartment: (A) upper layers, 0.6 mm and above, $n = 7$; (B) middle layers, 0.1–0.5 mm, $n = 5$; (C) deep layers, −0.1 mm and below, $n = 4$. (D–F) Same as (A–C), but for the binocular incongruent condition (red) compared to monocular (black). (G–I) Binocular modulation for the congruent (blue) and incongruent (red) conditions across the transient and sustained phases (abscissa) for the indicated laminar compartment; see (A–C). Diamonds represent means across neurons, error bars are the standard error of the mean, and dots show individual neurons; *n* differs from in (A–F), see Table 2).

the location of V1's granular input layer (Layer 4C; Figure 1D). Specifically, CSD analysis of visual responses to brief visual stimulation has been shown to reliably indicate the location of the primary geniculate input to V1 in the form of a distinct current sink that is thought to reflect combined excitatory postsynaptic potentials of the initial retinogeniculate volley of activation (Cox et al., 2017; Dougherty, Cox, Ninomiya, Leopold, & Maier, 2015; Maier, Adams, Aura, & Leopold, 2010; Maier, Aura, & Leopold, 2011; Mitzdorf, 1985). For each penetration with the laminar multielectrode array, CSD analysis was used to resolve this prominent initial current sink immediately following stimulus onset. The bottom of this sink was used as a marker of the transition between granular Layer 4C and the deeper Layer 5.

Thus, using this combination of criteria, each penetration was assigned three reference microelectrode contacts representing the top of V1, the Layer 4C/5 boundary, and the bottom of V1 (Figure 1D, "Align"). These points were used to align and average data across electrode penetrations and recording sessions, resulting in resolution of 0.1 ± 0.05 mm across V1's cortical depth.

Results

This study investigated the time course of laminar V1 spiking responses to monocular stimulation and binocular stimulation. In order to display stimuli independently to each eye, we had monkeys view a front-facing display through a mirror stereoscope while spiking activity was recorded with linear multielectrode arrays positioned across the layers of V1 (Figure 1A). We focused our study on the spiking activity of individually isolated V1 neurons, that is *single-unit activity* (see Methods and Table 1). We were interested in the response difference between a given neuron's preferred monocular stimulus displayed alone and the same stimulus with an additional stimulus in the other eye (binocular). The stimulus in the nondominant eye was either congruent (same orientation) or incongruent (orthogonal orientation) to the stimulus in the dominant eye. For binocular stimulation, we expect evoked

Downloaded from abstracts.iovs.org on 04/20/2024

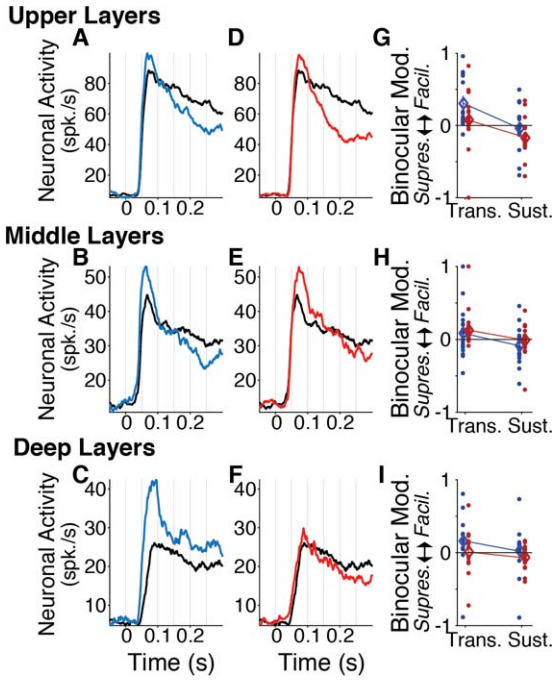

Figure 7. (A–C) Mean single-unit activity response to the binocular congruent (blue) and monocular (black) conditions across all tuned ocular-biased neurons as a function of laminar compartment: (A) upper layers, 0.6 mm and above, $n = 7$; (B) middle layers, 0.1–0.5 mm, $n = 5$; (C) deep layers, −0.1 mm and below, $n = 4$. (D–F) Same as (A–C), but for the binocular incongruent condition (red) compared to monocular (black). (G–I) Binocular modulation for the congruent (blue) and incongruent (red) conditions across the transient and sustained phases (abscissa) for the indicated laminar compartment; see (A–C). Diamonds are means across neurons, error bars are standard error of the mean, and dots show individual neurons; *n* differs from in (A–F), see Table 2).

responses to be either larger (facilitation), smaller (suppression), or the same compared to monocular stimulation (Figure 1B). As we were particularly interested in temporal dynamics, we considered two phases of V1 responses following stimulus onset, the initial transient (50–100 ms) and the sustained response (150–250 ms).

We performed all V1 electrode penetrations using linear microelectrode arrays. The relative depth of each microelectrode contact in cortex was determined using several neurophysiological criteria (Figure 1C and 1D) For each electrode penetration, the receptive-field location and tuning properties of the recorded neurons were characterized (Methods; Figure 2). The goal of this initial phase of the experiment was to identify the preferred orientation and ocularity of the recorded neurons so that the parameters of the main experiment could be customized to the neurons' response preferences (Figure 3A). We defined three main stimulus conditions:

- Monocular: Stimulus in the neuron's preferred (dominant) eye at the neuron's preferred orientation; no grating stimulus in nondominant eye (contrast = 0). In plots, shown in black.
- Binocular congruent: Dominant-eye stimulus set to the neuron's preferred orientation; nondominant-eye stimulus set to the neuron's preferred orientation. In plots, shown in blue.
- Binocular incongruent: Dominant-eye stimulus set to the neuron's preferred orientation; nondominant-eye stimulus oriented orthogonally to the neuron's preferred orientation. In plots, shown in red.

In all cases, the contrast of the stimulus in the dominant eye was about half that of the stimulus in the nondominant eye (typically 0.45 and 0.90 Michelson contrast, respectively; see Methods).

Tuning stimulus	Layers (figure)	Transient phase (50–100 ms)	Sustained phase (150–250 ms)
Equiocular congruent	Upper (6A)	$\Delta M = 9.04$, $t(7) = 2.53$, $p = 0.039$	$\Delta M = 0.19$, $t(7) = 0.07$, $p = 0.948$
	Middle (6B)	$\Delta M = 28.26$, $t(6) = 2.82$, $p = 0.030$	$\Delta M = 16.68$, $t(6) = 2.52$, $p = 0.046$
	Deep (6C)	$\Delta M = 36.23$, $t(5) = 2.11$, $p = 0.088$	$\Delta M = 14.56$, $t(5) = 1.20$, $p = 0.283$
Equiocular incongruent	Upper (6D)	$\Delta M = 2.95$, $t(6) = 1.96$, $p = 0.098$	$\Delta M = -3.24$, $t(6) = -1.22$, $p = 0.269$
	Middle (6E)	$\Delta M = 19.90$, $t(4) = 1.32$, $p = 0.256$	$\Delta M = 4.89$, $t(4) = 0.61$, $p = 0.576$
	Deep (6F)	$\Delta M = -6.93$, $t(3) = -0.85$, $p = 0.457$	$\Delta M = -3.73$, $t(3) = -1.58$, $p = 0.213$
Ocular-biased congruent	Upper (7A)	$\Delta M = 11.18$, $t(13) = 1.74$, $p = 0.105$	$\Delta M = -11.44$, $t(13) = -1.55$, $p = 0.145$
	Middle (7B)	$\Delta M = 7.44$, $t(19) = 2.15$, $p = 0.044$	$\Delta M = -3.54$, $t(19) = -2.52$, $p = 0.021$
	Deep (7C)	$\Delta M = 15.57$, $t(12) = 1.90$, $p = 0.082$	$\Delta M = 5.05$, $t(12) = 0.93$, $p = 0.370$
Ocular-biased incongruent	Upper (7D)	$\Delta M = 9.31$, $t(19) = 3.76$, $p = 0.001$	$\Delta M = -21.55$, $t(19) = -2.88$, $p = 0.010$
	Middle (7E)	$\Delta M = 7.34$, $t(18) = 2.10$, $p = 0.051$	$\Delta M = -1.42$, $t(18) = -1.08$, $p = 0.294$
	Deep (7F)	$\Delta M = -1.08$, $t(13) = -0.27$, $p = 0.789$	$\Delta M = -3.65$, $t(13) = -1.48$, $p = 0.162$

Table 2. Statistics by tuning, stimulus, layer, and temporal phase.

Downloaded from abstracts.iovs.org on 04/20/2024

Temporal dynamics of binocular V1 responses

First, we examined stimulus-evoked spiking responses, regardless of ocularity, tuning, and laminar position (Table 1; Figure 3B through 3G). The transient response evoked by both types of binocular stimuli exceeded that of the monocular stimulus—binocular congruent: $\Delta M = 13.73$ spikes/s over 50–100 ms, $t(90) = 5.44$, $p < 0.001$; binocular incongruent: $\Delta M = 5.85$ over 50–100 ms, $t(94) = 3.51$, $p = 0.001$. The congruent stimuli evoked an even greater response than the incongruent stimuli relative to monocular stimulation (see maximums in Figure 3B vs. Figure 3E). However, this period of binocular facilitation was limited to the transient phase of the visually evoked response (~50–100 ms, indicated in Figure 3B through 3G with the first pair of gray vertical lines). In the sustained response phase of the V1 spiking response (~150 ms and beyond, indicated in Figure 3B through 3G with the second pair of gray vertical lines), binocular facilitation decreased and eventually disappeared altogether—congruent: $\Delta M = 0.76$ over 150–250 ms, $t(90) = 0.38$, $p = 0.71$. Moreover, binocular responses to the incongruent stimuli were suppressed compared to monocular stimulation—incongruent (Figure 3E through 3G): $\Delta M = -5.57$ over 150–250 ms, $t(94) = -2.82$, $p < 0.05$—suggesting that the neural differentiation between binocular congruency and incongruency is expressed more dominantly during this phase.

We were curious how far this pattern of the V1 population response is representative of the spiking responses of individual neurons. To find out, we computed a normalized modulation index for each binocular stimulation condition compared to monocular stimulation (see Methods). Positive values of this binocular modulation index indicate facilitation and negative values indicate suppression of binocular responses relative to monocular responses. To capture temporal dynamics, we computed the binocular modulation index for both the transient (50–100 ms) and the sustained (150–250 ms) phases. Results are shown in Figure 3H and 3I. As expected from the population averages, we found that during the transient phase most neurons were facilitated when both eyes were stimulated (left histograms)—congruent: $M = 0.21$, $SD = 0.18$, $t(90) = 4.80$, $p < 0.001$; incongruent: $M = 0.11$, $SD = 0.36$, $t(94) = 3.006$, $p = 0.003$. By contrast, during the sustained phase only incongruent stimulation produced significant suppression across the population: $M = -0.06$, $SD = 0.29$, $t(94) = -2.01$, $p = 0.047$. The congruent condition trended negative but did not reach significance: $M = -0.02$, $SD = 0.34$, $t(90) = -0.548$, $p = 0.585$.

While V1 neurons on average showed greater transient responses for binocular stimulation that diminished during the sustained phase, there was considerable variability (see *SD*s just reported). We wondered if some of this variance could be explained by each neuron's ocularity (i.e., ocular dominance, or ocular preference). Our rationale was that a neuron's response bias for one or the other eye might be indicative of the relative strengths of each eye's inputs. Thus, the ocularity of a neuron might impact how it responds to simultaneous stimulation of both eyes. To explore this possibility, we correlated the binocular modulation index with a similar index of ocularity (Figure 4A through 4D). Larger ocularity index values indicate a greater response difference between the eyes. Smaller values indicate a more equivalent response between the eyes. Here too, we performed the analysis over both the transient (Figure 4A and 4B) and sustained (Figure 4C and 4D) phases. We found no significant relationship between a neuron's ocularity and the amount of binocular facilitation in the transient phase for either the congruent binocular condition (Figure 4A) $r(89) = -0.18$, $p = 0.08$, or the incongruent one (Figure 4B), $r(93) = -0.12$, $p = 0.28$. This suggests that the binocular facilitation observed in the transient phase is generally independent of a neuron's ocularity. Strikingly, this relationship changed during the sustained phase of the response (Figure 4C and 4D). Neurons with a stronger preference for one eye over the other tended to also exhibit more binocular suppression. This correlation between ocularity and binocular modulation was significant and negative for both the congruent condition (Figure 4C), $r(89) = -0.40$, $p < 0.001$, and the incongruent one (Figure 4D), $r(93) = -0.20$, $p < 0.05$. This suggests that a V1 neuron's sustained response to binocular stimulation is related to that neuron's ocularity, with neurons that show greater response differences between the eyes also exhibiting more binocular suppression.

On the other side of the ocularity spectrum—that is, the neurons that respond more equivalently between the two eyes—neurons appeared to be selectively facilitated when the stimuli matched between the eyes, as the intercept on the ordinate for the congruent condition was positive (0.15) while that for the incongruent condition was close to zero (0.02). This suggests a specialized role for neurons that have minimal response differences between the eyes in determining the congruency of binocular stimulation. To further explore this possibility, we decided to sort neurons based on their ocularity (Table 1). Specifically, we separated out the neurons that had equivalent responses between the eyes, which we termed equiocular, from those that exhibited significant response preferences for one eye over the other, which we termed ocular-biased. Note that all equiocular neurons showed a slight but insignificant difference in mean firing between the eyes, which allowed us to determine a

Downloaded from abstracts.iovs.org on 04/20/2024

preferred (dominant) and nonpreferred (nondominant) eye even for these unselective neurons. We also included neurons that showed no significant orientation tuning, all of which exhibited significant ocular preference, as a separate group. The population responses of each of these neuronal types, as well as the respective response differences between stimulation conditions, are shown in Figure 4E through 4J. As expected from the correlation analysis, there was a clear qualitative difference in the response patterns of all three groups of neurons.

Equiocular neurons (Figure 4E and 4F) exhibited significantly elevated responses for the congruent condition compared to the monocular condition in both the transient response phase, $\Delta M = 26.59$, $t(22) = 4.30$, $p < 0.001$, and the sustained one, $\Delta M = 12.12$, $t(22) = 2.66$, $p < 0.05$. However, this was not the case for the incongruent condition—transient: $\Delta M = 6.29$, $t(17) = 1.21$, $p = 0.243$; sustained: $\Delta M = -0.19$, $t(17) = -0.08$, $p = 0.94$. This observation suggests that equiocular neurons strongly differentiate between concordant and discordant stimuli across the eyes.

Ocular-biased neurons, on the other hand showed an inverse pattern of suppression rather than facilitation following the additive transient (Figure 4G and 4H). This decrease of binocular responses occurred for both congruent and incongruent stimuli, though the suppression for incongruent stimulation was both more pronounced (incongruent vs. monocular $\Delta M = -9.50$, compared to $\Delta M = -2.83$ for congruent vs. monocular) and more reliable across the population—incongruent: $t(55) = -3.11$, $p < 0.05$; congruent: $t(49) = -1.05$, $p = 0.30$. The congruent stimuli also evoked a slightly greater facilitative transient response than the incongruent stimuli, but this response difference was far less pronounced than for the equiocular neurons—congruent: $\Delta M = 11.90$, $t(49) = 3.68$, $p = 0.001$; incongruent: $\Delta M = 6.12$, $t(55) = 3.31$, $p < 0.05$. These findings suggest some level of inhibitory interaction among ocular-biased neurons during binocular stimulation.

Finally, we examined the response profiles of neurons that were untuned and ocular-biased (Figure 4I and 4J). The binocular responses for these neurons were largely comparable to their monocular responses throughout both the initial and transient phases—50–100 ms, congruent: $\Delta M = 2.37$, $t(17) = 1.44$, $p = 0.17$; incongruent: $\Delta M = 4.77$, $t(20) = 1.26$, $p = 0.22$; 150–250 ms, congruent: $\Delta M = -3.79$, $t(17) = -2.11$, $p = 0.05$; incongruent: $\Delta M = 0.32$, $t(20) = 0.15$, $p = 0.88$. Although both the sampling size and the firing rates of these neurons were rather low, this observation suggests that this population does not discriminate between monocular and binocular stimulation of any kind.

Laminar profile of V1 binocular response modulation

Neurons vary in many response properties across V1 layers, which is particularly relevant when it comes to binocular processing, because each eye's input arrives separately in the middle, granular layer (Layer 4C). We collected all of our data using linear microelectrode arrays. Consequently, we were able to identify the upper and lower bounds of V1 for each penetration as well as the bottom of Layer 4C using neurophysiological criteria (Methods; Figure 1D). Using these functionally defined cortical depth markers, we assigned each microelectrode contact, and the neurons recorded on each contact, a laminar location relative to the bottom of Layer 4C (Figure 5A). Then we examined the distribution of the binocular modulation index as a function of laminar location (Figure 5B and 5C). We observed that virtually all layers exhibited some binocular facilitation in the early, transient response phase when stimuli were congruent between the eyes (Figure 5B, dashed line). During the sustained response, binocular modulation decreased across all layers (Figure 5B, solid line).

Repeating the same analysis for the binocular incongruent condition revealed a different laminar pattern of activity. While this kind of stimulation also caused transient binocular enhancement (Figure 5C, dashed line), this response enhancement was mostly confined to the middle and upper layers (0.0–1.2 mm above the 4C/5 boundary). To our surprise, the deep layers (0.7 to 0.0 mm *below* the 4C/5 boundary) exhibited response suppression during the initial transient. During the sustained phase, binocular suppression prevailed (Figure 5C, solid line). To better understand these laminar differences in processing binocular stimuli, we next looked at the population response of both the equiocular and ocular-biased neurons within the upper, supragranular layers (0.6 mm and above), the middle, granular layers (0.1–0.5 mm), and the deep, infragranular layers (–0.1 mm and below). Figure 6A through 6C shows the layer-specific responses of equiocular V1 neurons. Binocular congruent stimulation evoked significantly greater activation of the granular input neurons than stimulation of one eye alone, which persisted throughout both the transient part of the response, $\Delta M = 28.26$, $t(6) = 2.82$, $p < 0.05$, and the sustained part, $\Delta M = 16.68$, $t(6) = 2.52$, $p < 0.05$ (Figure 6B). This finding makes sense in that equiocular neurons within V1's input layer might receive balanced net excitation from either eye.

However, equiocular neurons in both the upper layers (Figure 6A) and the deep layers (Figure 6C) showed binocular facilitation only during the transient phase—upper: $\Delta M = 9.04$, $t(7) = 2.53$, $p < 0.05$; deep: $\Delta M = 36.23$, $t(5) = 2.11$, $p = 0.088$. Once these neurons

Downloaded from abstracts.iovs.org on 04/20/2024

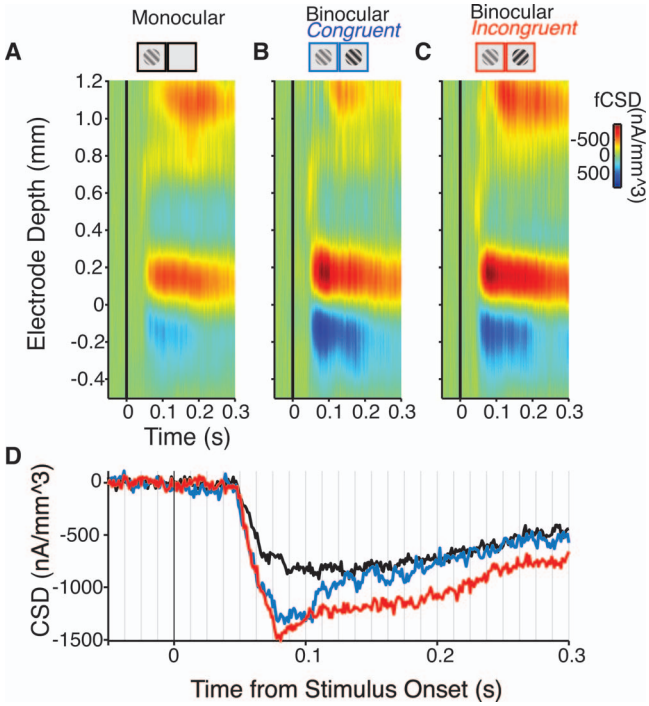

Figure 8. (A) Current source density evoked by monocular stimulation across all penetrations where both binocular conditions were collected ($N = 22$) as a function of time (abscissa, 0 = stimulus onset). Data are smoothed in two dimensions ($\sigma = 35$ ms and 0.18 mm). (B) Same as (A), but for the binocular congruent condition. (C) Same as (A), but for the binocular incongruent condition. (D) Initial sink (mean current source density from 0.1 to 0.2 mm) evoked by the monocular (black), binocular congruent (blue), and binocular incongruent (red) conditions.

reached the sustained phase, there was little difference between the monocular and binocular responses—upper: $\Delta M = 0.19$, $t(7) = 0.07$, $p = 0.95$; deep: $\Delta M = 14.56$, $t(5) = 1.20$, $p = 0.28$. In other words, while equiocular neurons in V1's input layer fire almost twice as much when both eyes are stimulated rather than one, the equiocular neurons in all other layers do so only briefly, before reaching a response that resembles that of a monocular view.

Interestingly, the same equiocular neurons responded somewhat differently when the binocular stimuli were incongruent (Figure 6D through 6F). Specifically, there was an overall diminished response during the transient phase in the upper and deep layers. And the sustained response across all layers resembled that of monocular stimulation (see Figure 6G through 6I and Table 2 for summary statistics). These observations combined point at laminar specialization for the transient binocular facilitation of the population response.

We repeated the same analysis for the ocular-biased neurons (Figure 7, Table 2). In the middle layers, both binocular congruent and binocular incongruent stimuli first evoked binocular facilitation and then resulted in binocular suppression. This response pattern was mirrored in the upper layers. Ocular-biased neurons in the deep layers, however, showed an interesting idiosyncratic response. Specifically, they exhibited binocular facilitation throughout the response if stimuli were congruent, but barely differentiated between monocular and binocular stimulation if stimuli were incongruent. Importantly, the overall pattern of a transient response enhancement for binocular stimuli followed by stimulus-specific suppression or facilitation prevailed for this class of neurons.

Temporal evolution of laminar CSD

So far we have only evaluated the spiking output across V1's laminar microcircuit. Linear microelectrode arrays can also be used to measure the spatiotemporal profile of synaptic inputs. This can be achieved by converting the slow-varying extracellular voltages of the LFP into time-varying current sinks and sources (CSD; see Methods). Figure 8A through 8C shows the CSD response to monocular and binocular stimulation, respectively. Red areas indicate current influx, or net depolarization, in that region (current sink; negative by convention). Of particular interest for this study is the first current sink following stimulus onset in the middle, granular layers, which is thought to reflect the initial volley of geniculocortical activation. This initial current sink was larger (i.e., more negative) for both congruent and incongruent stimulation. This is in line with the fact that synaptic activity in V1 might increase when layers in the lateral geniculate nucleus that are innervated by either eye are activated.

Closer examination of the initial sink (Figure 8D) revealed that the initial deflections evoked by both types of binocular stimuli were not significantly different from each other—from 50 to 100 ms, $t(37) = -0.64$, $p = 0.53$—though they were both significantly larger compared to the monocular response—congruent: $\Delta M = -480$ nA/mm^2, $t(37) = -2.79$, $p < 0.05$; incongruent: $\Delta M = -495$, $t(41) = -4.168$, $p < 0.001$. However, the current sink for the congruent stimuli slowly approached the activation level of the monocular stimulus—from 150 to 250 ms, $\Delta M = -165.55$, $t(37) = -0.98$, $p = 0.33$—while the current sink for the incongruent stimuli remained significantly greater than that of the monocular stimulus—from 150 to 250 ms, $\Delta M = -337$, $t(41) = -3.15$, $p < 0.05$. Assuming that the initial sink is indicative of synaptic activation, it thus seems that inputs to the granular layer gradually normalize congruent binocular responses to match those of monocular viewing. By contrast, synaptic responses to incongruent stimuli never approach those

Downloaded from abstracts.iovs.org on 04/20/2024

of monocular stimulation. This finding suggests that interocular concordance versus discordance differentially affects even synaptic activity in V1's input layer.

Discussion

We found that the temporal dynamics of V1 responses to congruent and incongruent binocular stimulation are indicative of a series of computational steps that the visual system employs in processing both concordant and discordant views of the two eyes. Across the population, both V1 neurons that were significantly selective for one eye and those that were driven by each eye equally initially responded more vigorously when both eyes were stimulated, suggesting some form of (subadditive) binocular summation. About 150 ms following this initial binocular facilitation, both groups of neurons exhibited a relative decrease in response magnitude. However, widespread V1 response suppression only occurred if the stimuli in the two eyes were of orthogonal orientation (incongruent), thus posing significant interocular conflict. Neurons with significant response preference for one eye over the other also trended towards binocular suppression when the stimuli in the two eyes were of the same orientation (congruent). However, binocularly driven neurons that lacked significant ocular preference (equiocular neurons) showed the opposite pattern, in the form of sustained binocular summation when both eyes were stimulated congruently. Taken together, these results suggest that following an initial boost in firing caused by stimulation of both eyes rather than one, V1 neurons rapidly differentiate between congruent and incongruent stimulation across the two eyes, resulting in widespread reduction of visual responses when interocular conflict arises. As discussed later, this transition from response enhancement during the transient phase to response reduction during the sustained phase may serve as an initiator for secondary mechanisms of interocular conflict resolution, such as binocular rivalry.

Relation to previous dCOS literature

The comparisons between the binocular incongruent and monocular stimulation conditions in this study are comparable to those between the stimulation conditions for the previously described phenomenon of dichoptic cross-orientation suppression (dCOS). The vast majority of work on dCOS has been carried out in area 17 of anesthetized cats (Sengpiel et al., 1998; Sengpiel & Blakemore, 1994; Sengpiel, Freeman & Blakemore, 1995; Sengpiel & Vorobyov, 2005; Walker, Ohzawa, & Freeman, 1998). Although the anatomical organization of binocular vision differs significantly between cats and primates (Dougherty et al., 2018; Heesy, Kamilar & Willms, 2011; Hendrickson et al., 1978; Wilson & Cragg, 1967; Yoshioka, Blasdel, Levitt, & Lund, 1996), area 17 in the cat and V1 in primates are generally considered functionally homologous. To a first approximation, our data reveal that dCOS occurs in primates to a similar degree as in cats. Previous studies have suggested that dCOS is mediated by intracortical inhibition (Sengpiel & Vorobyov, 2005). This conclusion was based on the observation that dCOS exhibits differential contrast-gain control compared to monocular cross-orientation suppression, dCOS's sensitivity to visual adaptation to the rate of stimulus motion, and the ability to extinguish dCOS with a GABA antagonist in area 17. Our finding that neurons outside V1's main retinogeniculate input layer exhibit the strongest orientation-specific binocular suppression corroborates the view that dCOS arises from intracortical interactions, although CSD analysis suggests that the granular input layers are involved as well. Our findings in V1 also agree with cat studies on the frequency of dCOS across neurons, with over 50% of our neurons exhibiting suppression after ~150 ms, as well as the magnitude of suppression, which hovered around 10 spikes/s (Sengpiel et al., 1998). Another study in anesthetized macaques has reported similar percentages (Endo et al., 2000), providing further support that application of anesthetics does not significantly alter this fundamental mechanism.

Relation to binocular rivalry

Another popular approach to studying binocular integration on the level of single neurons in visual cortex has been binocular rivalry (for reviews, see Leopold, 2012; Logothetis, 1998; Schmid & Maier, 2015). In fact, most models of binocular suppression are designed to specifically account for perceptual alternations in binocular rivalry (Grossberg, Yazdanbakhsh, Cao, & Swaminathan, 2008), and generally postulate competition between neurons encoding each eye, mediated by reciprocal inhibition between eye-specific neuronal populations (Blake & Wilson, 2011; Brascamp, Sohn, Lee, & Blake, 2013; Tong et al., 2006).

However, neuronal correlates of binocular rivalry are defined differently than dCOS. In binocular rivalry, spiking responses are studied relative to the subject's perceptual experience (Bahmani, Murayama, Logothetis, & Keliris, 2014; Fries, Roelfsema, Engel, König, & Singer, 1997; Gail et al., 2004; Leopold & Logothetis, 1996; Macknik & Martinez-Conde, 2004; Maier et al., 2007; Maier, Panagiotaropoulos, Tsuchiya, & Keliris, 2012; Maier et al., 2008; Polonsky et al., 2000;

Downloaded from abstracts.iovs.org on 04/20/2024

Sheinberg & Logothetis, 1997; Wilke, Mueller, & Leopold, 2009; Wunderlich, Schneider, & Kastner, 2005). That is, the neuronal signals are typically investigated in order to identify populations of neurons that correlate with the fluctuating percept during interocular conflict. The general assumption of these studies is that the population of neurons representing the nonperceived stimulus are suppressed. In contrast, dCOS is defined from a neuron's perspective, such that all comparisons are to that neuron's preferred stimulus and dominant eye and thus agnostic to perception (Endo et al., 2000; Sengpiel & Blakemore, 1994; Sengpiel, Freeman, & Blakemore, 1995; Sengpiel & Vorobyov, 2005). Across V1, there are neurons that prefer each combination of eye and stimulus orientation. Thus, for any given binocular incongruent stimulus, dCOS will cause widespread response reduction among all neurons representing both eyes as well as both stimuli. If sensory drive from the two eyes is balanced between the eyes—as is characteristic for normal, unaltered vision (for interesting exceptions, see Wilke et al., 2003; Wolfe, 1984; Yang, Heeger, Blake, & Seidemann, 2015)—then dCOS does not favor either eye or stimulus at the population level. Instead, dCOS remains constant while perception fluctuates between the two eyes' views. This invariance supports the supposition that dCOS is a fundamental neuronal computation that is not linked directly to the perceptual outcome of ongoing binocular rivalry alternations.

One intriguing possibility is that dCOS could serve as a signaling mechanism of binocular conflict that precedes and ultimately paves the way for binocular rivalry alternations (Baker, Meese, & Summers, 2007; Sengpiel et al., 1998; Sengpiel, Blakemore, & Harrad, 1995). Since perceptual binocular rivalry is not instantaneous but requires at least 150 ms of exposure (Wolfe, 1983), the timing of onset of its onset is well matched to the two distinct phases of binocular integration reported here. Specifically, it seems that the initiation of response reduction for binocular incongruent stimuli is more or less coincident with the initiation of perceptual alternation in binocular rivalry. This finding lends support for the hypothesis that the onset of dCOS is related to the initiation of binocular rivalry.

Response dynamics in V1

We still know little about how cortical areas are organized in the temporal domain (Murray et al., 2014). Temporal response characteristics of V1 neurons have been studied extensively in the context of orientation tuning (Celebrini, Thorpe, Trotter, & Imbert, 1993; Ringach et al., 1997), where inhibition rapidly follows excitation to increase orientation selectivity (Ringach et al., 2003; Shapley, Hawken, & Ringach, 2003; but see Mazer, Vinje, McDermott, Schiller, & Gallant, 2002). For the neuronal response dynamics reported here, response reduction for binocular stimuli emerges within ~150 ms of the initial transient. One interpretation is that this initial response, where activity for binocular stimulation exceeds the magnitude of monocular stimulation, is driven predominately by feed-forward excitation, while the subsequent response reduction for binocular stimulation is a result of cortical-cortical inhibition. This inhibition could be mediated by short-range horizontal connections between neighboring ocular dominance columns. While long-range (>0.5 mm) horizontal connections in the upper layers of primate V1 tend to be homophilic for ocular dominance and orientation, short-range (<0.5 mm) horizontal connections are dense and more promiscuous (Malach et al., 1993; Stettler, Das, Bennett, & Gilbert, 2002; Yoshioka et al., 1996). However, the observation that congruent binocular stimuli evoked response enhancement in some V1 neurons suggests that interocular inhibition is either bypassed or superseded. The functional differences between equiocular and ocular-biased neurons suggest that each group receives different input from the two eyes, with equiocular neurons receiving nearly equivalent net excitatory drive from each of the two eyes.

Laminar differences in binocular processing

The evolution of binocular signals across the V1 microcircuit is particularly informative regarding the sequence of computational processes underlying integration of the two eyes' signals, especially in view of the classic canonical microcircuit model. According to this model, visual information flows from the granular input layer (Layer 4, or Layer 4C in primates) to upper layers (Layers 2/3) and then to the deep layers (Layers 5/6; Callaway, 1998; Douglas & Martin, 2004). We found that neurons in both the middle granular layer and the upper layers of V1 exhibited early enhancement for incongruent binocular stimulation, while neurons in the deep layers did not. The observation of rapid, almost immediate, emergence of binocular suppression to incongruent stimuli in the deep layers is puzzling. The canonical microcircuit model assumes a strict order of sequential processing starting in Layer 4C, with higher order computations emerging at subsequent processing steps in the layers above and below. However, lateral geniculate nucleus neurons branch before reaching Layer 4C, and these axon collaterals directly innervate V1's Layer 6 (Briggs, 2010). One possibility is that this retinogeniculate activation bypassing Layer 4C instigates the computation of

Downloaded from abstracts.iovs.org on 04/20/2024

binocular suppression in the deep layers ahead of other laminar compartments. Another interpretation is that binocular suppression in the deep layers is established immediately following sensory activation of middle and upper layers. In other words, the first population of neurons enacting binocular suppression could be neurons in the deep layers that receive input from neurons in the upper layers. Binocular suppression in the deep layers then propagates to the upper layers, via interlaminar connections (Dougherty et al., 2015; Spaak, Bonnefond, Maier, Leopold, & Jensen, 2012). This order of excitement and inhibition within V1's laminar microcircuit suggests that cortico-cortical interactions mediate binocular suppression within V1, with each portion of the microcircuit playing a distinct role. These findings provide important new information for neuronal models of binocular processing (Bhaumik & Shah, 2014; Bridge & Cumming, 2008).

Limitations

It is worth noting that all congruent binocular stimuli used in this study were at or near zero disparity. This is important since V1 neurons are sensitive to interocular disparity (Cumming & DeAngelis, 2001), and binocular modulation changes with disparity. More work will be needed to extend and generalize the current results to a broader range of interocular disparities. We also would like to note that some of our sample sizes were necessarily small and drawn from predominantly one of two moneys. Another limitation of note is that our spatial resolution is limited. In addition to the 100-μm interelectrode spacing of the linear array, we introduce a ±50-μm sampling error whenever we align the data across individual sessions (see Methods). Microelectrodes have been shown to pick up single-neuron activity from soma that are up to 500 μm distant from the electrode contact (Buzsáki, Anastassiou, & Koch, 2012). However, our spike-sorting approach is specifically designed to take advantage of the multielectrode array to resolve spikes that span multiple electrode contacts. The past couple of years have witnessed encouraging new developments for high-density electrodes, such as the Neuropixel arrays with a spacing of 20 μm or better. These multielectrode arrays can simultaneously capture spikes on multiple nearby electrode contacts, resulting in more precise localization of the neurons of origin. It would be of great interest to repeat our study once laminar neurophysiology with this superior spatial resolution is readily available in primates. Higher cell counts per laminar penetration will also alleviate statistical issues associated with the relatively small sample size resulting from splitting neurons into numerous neuronal cell types per laminar compartment. Due to this limitation of our study, we opted to show individual unit data in addition to group statistics wherever appropriate. However, we caution the reader that some of our conclusions regarding the functional organization of V1 circuitry rest on a rather small number of neurons within each laminar compartment.

Conclusions

Our eyes provide two streams of information that are merged in the primary visual cortex (V1). Here we show that V1 spiking responses to stimulation of both eyes are indicative of a multistage process of binocular combination, with an early phase of general excitation followed by more pronounced stimulus-dependent processing. These results provide important new insights into the neural machinery that supports the combination of the two eyes' perspectives into a single coherent view.

Keywords: binocular vision, microcircuit, macaque, binocular rivalry, interocular suppression

Acknowledgments

The authors would like to thank S. Amemori, Dr. T. Apple, Dr. P. Balaram, M. Feurtado, K. George-Durrett, A. Graybiel, N. Halper, P. Henry, M. Johnson, Dr. C. Jones, M. Maddox, L. McIntosh, Dr. A. Newton, J. Parker, C. Thompson, K. Torab, C. Subraveti, B. Williams, and R. Williams for technical advice and assistance; and Dr. R. Krauzlis, Dr. F. Tong, Dr. K. Dieter, B. M. Carlson, and N. Valov for comments on previous drafts of this manuscript. This work was supported by a research grant to AM from the National Eye Institute (1R01EY027402-01). KD and JAW were each supported by a National Eye Institute Training Grant (5T32EY007135-23). AM was supported by a research grant of the Whitehall Foundation, a Career Starter grant from the Knights Templar Eye Foundation, and a Fellowship of the Alfred P. Sloan Foundation. MAC, KD, and AM conceptualized and designed the study; MAC, KD, and MSS trained the animals and implemented the experiments; AM, MAC, JAW, and KD collected and analyzed neurophysiological data; MAC prepared figures for publication; and AM and MAC wrote the manuscript with input from other authors. The authors declare no competing financial interests.

Commercial relationships: none.
Corresponding author: Alexander Maier.
Email: alex.maier@vanderbilt.edu.

Downloaded from abstracts.iovs.org on 04/20/2024

Address: Department of Psychology, College of Arts and Science, Vanderbilt Vision Research Center, Center for Cognitive and Integrative Neuroscience, Vanderbilt University, Nashville, TN, USA.

References

Asaad, W. F., & Eskandar, E. N. (2008). A flexible software tool for temporally-precise behavioral control in Matlab. *Journal of Neuroscience Methods*, *174*(2), 245–258.

Asaad, W. F., Santhanam, N., McClellan, S., & Freedman, D. J. (2013). High-performance execution of psychophysical tasks with complex visual stimuli in MATLAB. *Journal of Neurophysiology*, *109*(1), 249–260.

Bahmani, H., Murayama, Y., Logothetis, N. K., & Keliris, G. A. (2014). Binocular flash suppression in the primary visual cortex of anesthetized and awake macaques. *PLoS One*, *9*(9), e107628.

Baker, D. H., Meese, T. S., & Summers, R. J. (2007). Psychophysical evidence for two routes to suppression before binocular summation of signals in human vision. *Neuroscience*, *146*(1), 435–448.

Bhaumik, B., & Shah, N.P. (2014). Development and matching of binocular orientation preference in mouse V1. *Frontiers in Systems Neuroscience*, *8*, 128.

Bishop, P. O., Burke, W., & Davis, R. (1959, August 28). Activation of single lateral geniculate cells by stimulation of either optic nerve. *Science*, *130*(3374), 506–507.

Blake, R., & Fox, R. (1973). The psychophysical inquiry into binocular summation. *Perception & Psychophysics*, *14*(1), 161–185.

Blake, R., & Logothetis, N. K. (2002). Visual competition. *Nature Reviews Neuroscience*, *3*(1), 13–21.

Blake, R., & Wilson, H. (2011). Binocular vision. *Vision Research*, *51*(7), 754–770.

Brascamp, J., Sohn, H., Lee, S.-H., & Blake, R. (2013). A monocular contribution to stimulus rivalry. *Proceedings of the National Academy of Sciences, USA*, *110*(21), 8337–8344.

Bridge, H., & Cumming, B.G. (2008). Representation of binocular surfaces by cortical neurons. *Current Opinion in Neurobiology*, *18*, 425–430.

Briggs, F. (2010). Organizing principles of cortical layer 6. *Frontiers in Neural Circuits*, *4*, 3.

Buzsáki, G., Anastassiou, C. A., & Koch, C. (2012). The origin of extracellular fields and currents—EEG, ECoG, LFP and spikes. *Nature Reviews Neuroscience*, *6*, 407–420.

Callaway, E. M. (1998). Local circuits in primary visual cortex of the macaque monkey. *Annual Review of Neuroscience*, *21*(1), 47–74.

Carmel, D., Arcaro, M., Kastner, S., & Hasson, U. (2010). How to create and use binocular rivalry. *JoVE (Journal of Visualized Experiments)*, (45): e2030.

Carter, O., & Cavanagh, P. (2007). Onset rivalry: Brief presentation isolates an early independent phase of perceptual competition. *PLoS One*, *2*(4), e343.

Casagrande, V. A., & Boyd, J. D. (1996). The neural architecture of binocular vision. *Eye*, *10*(2), 153–160.

Celebrini, S., Thorpe, S., Trotter, Y., & Imbert, M. (1993). Dynamics of orientation coding in area V1 of the awake primate. *Visual Neuroscience*, *10*(5), 811–825.

Cox, M. A., Dougherty, K., Adams, G. K., Reavis, E. A., Westerberg, J. A., Moore, B. S., Leopold, D. A., & Maier, A. (2017). Spiking suppression precedes cued attentional enhancement of neural responses in primary visual cortex. *Cerebral Cortex*, *97*(2), 1–14.

Cox, M. A., Schmid, M. C., Peters, A. J., Saunders, R. C., Leopold, D. A., & Maier, A. (2013). Receptive field focus of visual area V4 neurons determines responses to illusory surfaces. *Proceedings of the National Academy of Sciences, USA*, *110*(42), 17095–17100.

Cumming, B. G., & DeAngelis, G. C. (2001). The physiology of stereopsis. *Annual Review of Neuroscience*, *24*(1), 203–238.

Dougherty, K., Cox, M. A., Ninomiya, T., Leopold, D. A., & Maier, A. (2017). Ongoing alpha activity in V1 regulates visually driven spiking responses. *Cerebral Cortex*, *27*(2), 1113–1124.

Dougherty, K., Schmid, M. C., & Maier, A. (2019). Binocular response modulation in the lateral geniculate nucleus. *Journal of Comparative Neurology*, *527*(3), 522–534.

Douglas, R. J., & Martin, K. A. C. (2004). Neuronal circuits of the neocortex. *Annual Review of Neuroscience*, *27*(1), 419–451.

Endo, M., Kaas, J. H., Jain, N., Smith, E. L., & Chino, Y. (2000). Binocular cross-orientation suppression in the primary visual cortex (V1) of infant rhesus monkeys. *Investigative Ophthalmology & Visual Science*, *41*(12), 4022–4031.

Fries, P., Roelfsema, P. R., Engel, A. K., König, P., &

Downloaded from abstracts.iovs.org on 04/20/2024

Singer, W. (1997) Synchronization of oscillatory responses in visual cortex correlates with perception in interocular rivalry. *Proceedings of the National Academy of Sciences, USA*, *94*(23), 12699–12704.

Gail, A., Brinksmeyer, H. J., & Eckhorn, R. (2004). Perception-related modulations of local field potential power and coherence in primary visual cortex of awake monkey during binocular rivalry. *Cerebral Cortex*, *14*(3), 300–313.

Grossberg, S., Yazdanbakhsh, A., Cao, Y., & Swaminathan, G. (2008). How does binocular rivalry emerge from cortical mechanisms of 3-D vision? *Vision Research*, *48*(21), 2232–2250.

Hanes, D. P., Thompson, K. G., & Schall, J. D. (1995). Relationship of presaccadic activity in frontal eye field and supplementary eye field to saccade initiation in macaque: Poisson spike train analysis. *Experimental Brain Research*, *103*(1), 85–96.

Heesy, C. P. (2004). On the relationship between orbit orientation and binocular visual field overlap in mammals. *The Anatomical Record Part A: Discoveries in Molecular, Cellular, and Evolutionary Biology*, *281*(1), 1104–1110.

Heesy, C. P., Kamilar, J. M., & Willms, J. (2011). Retinogeniculostriate pathway components scale with orbit convergence only in primates and not in other mammals. *Brain, Behavior and Evolution*, *77*(2), 105–115.

Hendrickson, A. E., Wilson, J. R., & Ogren, M. P. (1978). The neuroanatomical organization of pathways between the dorsal lateral geniculate nucleus and visual cortex in Old World and New World primates. *The Journal of Comparative Neurology*, *182*(1), 123–136.

Howard, I. P. (2012). *Perceiving in depth, vol. 1: Basic mechanisms*. Oxford, UK: Oxford University Press.

Howard, I. P., & Rogers, B. J. (2012). *Perceiving in depth, vol. 2: Stereoscopic Vision*. Oxford, UK: Oxford University Press.

Hubel, D. H., & Freeman, D. C. (1977). Projection into the visual field of ocular dominance columns in macaque monkey. *Brain Research*, *122*(2), 336–343.

Hubel, D. H., & Wiesel, T. N. (1968). Receptive fields and functional architecture of monkey striate cortex. *The Journal of Physiology*, *195*(1), 215–243.

Jones, R. K., & Lee, D. N. (1981). Why two eyes are better than one: the two views of binocular vision. *Journal of Experimental Psychology. Human Perception and Performance*, *7*(1), 30–40.

Kato, H., Bishop, P. O., & Orban, G. A. (1981). Binocular interaction on monocularly discharged lateral geniculate and striate neurons in the cat. *Journal of Neurophysiology*, *46*(5), 932–951.

Katyal, S., He, S., & Engel, S. (2015). Adapting the mechanism that initiates binocular rivalry. *Journal of Vision*, *15*(12): 274, https://doi.org/10.1167/15.12.274. [Abstract]

Keliris, G. A., Logothetis, N. K., & Tolias, A. S. (2010). The role of the primary visual cortex in perceptual suppression of salient visual stimuli. *PLoS Biology*, *30*(37), 12353–12365.

Knapen, T., Brascamp, J., Pearson, J., van Ee, R., & Blake, R. (2011). The role of frontal and parietal brain areas in bistable perception. *The Journal of Neuroscience*, *31*(28), 10293–10301.

Kumagami, T., Zhang, B., Smith, E. L., & Chino, Y. M. (2000). Effect of onset age of strabismus on the binocular responses of neurons in the monkey visual cortex. *Investigative Ophthalmology & Visual Science*, *41*(3), 948–954.

Lee, S.-H., Blake, R., & Heeger, D. J. (2005). Traveling waves of activity in primary visual cortex during binocular rivalry. *Nature Neuroscience*, *8*(1), 22–23.

Leopold, D. A. (2012). Primary visual cortex: Awareness and blindsight. *Annual Review of Neuroscience*, *35*(1), 91–109.

Leopold, D. A., & Logothetis, N. K. (1996, February 8). Activity changes in early visual cortex reflect monkeys' percepts during binocular rivalry. *Nature*, *379*(6565), 549–553.

Logothetis, N. K. (1998). Single units and conscious vision. *Philosophical Transactions of the Royal Society of London, Series B: Biological Sciences*, *353*(1377), 1801–1818.

Logothetis, N. K., Kayser, C., & Oeltermann, A. (2007). In vivo measurement of cortical impedance spectrum in monkeys: Implications for signal propagation. *Neuron*, *55*(5), 809–823.

Macknik, S. L., & Martinez-Conde, S. (2004). Dichoptic visual masking reveals that early binocular neurons exhibit weak interocular suppression: Implications for binocular vision and visual awareness. *Journal of Cognitive Neuroscience*, *16*(6), 1049–1059.

Maier, A., Adams, G. K., Aura, C., & Leopold, D. A. (2010). Distinct superficial and deep laminar domains of activity in the visual cortex during rest and stimulation. *Frontiers in Systems Neuroscience*, *4*:e31.

Maier, A., Aura, C. J., & Leopold, D. A. (2011). Infragranular sources of sustained local field potential responses in macaque primary visual

Downloaded from abstracts.iovs.org on 04/20/2024

cortex. *The Journal of Neuroscience*, *31*(6), 1971–1980.

Maier, A., Logothetis, N. K., & Leopold, D. A. (2007). Context-dependent perceptual modulation of single neurons in primate visual cortex. *Proceedings of the National Academy of Sciences, USA*, *104*(13), 5620–5625.

Maier, A., Panagiotaropoulos, T. I., Tsuchiya, N., & Keliris, G. A. (2012). Introduction to research topic—binocular rivalry: A gateway to studying consciousness. *Frontiers in Human Neuroscience*, *6*, 263.

Maier, A., Wilke, M., Aura, C., Zhu, C., Ye, F. Q., & Leopold, D. A. (2008). Divergence of fMRI and neural signals in V1 during perceptual suppression in the awake monkey. *Nature Neuroscience*, *11*(10), 1193–1200.

Malach, R., Amir, Y., Harel, M., & Grinvald, A. (1993). Relationship between intrinsic connections and functional architecture revealed by optical imaging and in vivo targeted biocytin injections in primate striate cortex. *Proceedings of the National Academy of Sciences, USA*, *90*(22), 10469–10473.

Mazer, J. A., Vinje, W. E., McDermott, J., Schiller, P. H., & Gallant, J. L. (2002). Spatial frequency and orientation tuning dynamics in area V1. *Proceedings of the National Academy of Sciences, USA*, *99*(3), 1645–1650.

Mitzdorf, U. (1985). Current source-density method and application in cat cerebral cortex: Investigation of evoked potentials and EEG phenomena. *Physiological Reviews*, *65*(1), 37–100.

Murray, J. D., Bernacchia, A., Freedman, D. J., Romo, R., Wallis, J. D., Cai, X., ... Wang, X. J. (2014). A hierarchy of intrinsic timescales across primate cortex. *Nature Neuroscience*, *17*(12), 1661–1663.

Nauhaus, I., Nielsen, K. J., & Callaway, E. M. (2016). Efficient receptive field tiling in primate V1. *Neuron*, *91*(4), 893–904.

Nauhaus, I., Nielsen, K. J., Disney, A. A., & Callaway, E. M. (2012). Orthogonal micro-organization of orientation and spatial frequency in primate primary visual cortex. *Nature Neuroscience*, *12*, 1683–1690.

Nicholson, C., & Freeman, J. A. (1975). Theory of current source-density analysis and determination of conductivity tensor for anuran cerebellum. *Journal of Neurophysiology*, *38*(2), 356–368.

Pachitariu, M., Steinmetz, N., Kadir, S., Carandini, M., & Harris, K. D. (2016). Kilosort: Realtime spike-sorting for extracellular electrophysiology with hundreds of channels. *bioRxiv*, 061481.

Panagiotaropoulos, T. I., Deco, G., Kapoor, V., & Logothetis, N. K. (2012). Neuronal discharges and gamma oscillations explicitly reflect visual consciousness in the lateral prefrontal cortex. *Neuron*, *74*(5), 924–935.

Polonsky, A., Blake, R., Braun, J., & Heeger, D. J. (2000). Neuronal activity in human primary visual cortex correlates with perception during binocular rivalry. *Nature Neuroscience*, *3*(11), 1153–1159.

Qian, C. S., & Brascamp, J. W. (2017). How to build a dichoptic presentation system that includes an eye tracker. *Journal of Visualized Experiments*, *2017*(127):e56033.

Ringach, D. L., Hawken, M. J., & Shapley, R. (1997, May 15). Dynamics of orientation tuning in macaque primary visual cortex. *Nature*, *387*(6630), 281–284.

Ringach, D. L., Hawken, M. J., & Shapley, R. (2003). Dynamics of orientation tuning in macaque V1: The role of global and tuned suppression. *Journal of Neurophysiology*, *90*(1), 342–352.

Sayer, R. J., Friedlander, M. J., & Redman, S. J. (1990). The time course and amplitude of EPSPs evoked at synapses between pairs of CA3/CA1 neurons in the hippocampal slice. *The Journal of Neuroscience*, *10*(3), 826–836.

Schmid, M. C., & Maier, A. (2015). To see or not to see—Thalamo-cortical networks during blindsight and perceptual suppression. *Progress in Neurobiology*, *126*, 36–48.

Schmiedt, J. T., Maier, A., Fries, P., Saunders, R. C., Leopold, D. A., & Schmid, M. C. (2014). Beta oscillation dynamics in extrastriate cortex after removal of primary visual cortex. *The Journal of Neuroscience*, *34*(35), 11857–11864.

Sengpiel, F., Baddeley, R. J., Freeman, T. C., Harrad, R., & Blakemore, C. (1998). Different mechanisms underlie three inhibitory phenomena in cat area 17. *Vision Research*, *38*(14), 2067–2080.

Sengpiel, F., & Blakemore, C. (1994, April 28). Interocular control of neuronal responsiveness in cat visual cortex. *Nature*, *368*(6474), 847–850.

Sengpiel, F., Blakemore, C., & Harrad, R. (1995). Interocular suppression in the primary visual cortex: A possible neural basis of binocular rivalry. *Vision Research*, *35*(2), 179–195.

Sengpiel, F., Freeman, T. C., & Blakemore, C. (1995). Interocular suppression in cat striate cortex is not orientation selective. *NeuroReport*, *6*(16), 2235–2239.

Sengpiel, F., & Vorobyov, V. (2005). Intracortical origins of interocular suppression in the visual

Downloaded from abstracts.iovs.org on 04/20/2024

cortex. *The Journal of Neuroscience*, *25*(27), 6394–6400.

Shapley, R., Hawken, M., & Ringach, D. L. (2003). Dynamics of orientation selectivity in the primary visual cortex and the importance of cortical inhibition. *Neuron*, *38*(5), 689–699.

Sheinberg, D. L., & Logothetis, N. K. (1997). The role of temporal cortical areas in perceptual organization. *Proceedings of the National Academy of Sciences, USA*, *94*(7), 3408–3413.

Smith, E. L., Chino, Y. M., Ni, J., Cheng, H., Crawford, M. L., & Harwerth, R. S. (1997). Residual binocular interactions in the striate cortex of monkeys reared with abnormal binocular vision. *Journal of Neurophysiology*, *78*(3), 1353–1362.

Spaak, E., Bonnefond, M., Maier, A., Leopold, D. A., & Jensen, O. (2012). Layer-specific entrainment of γ-band neural activity by the α rhythm in monkey visual cortex. *Current Biology*, *22*(24), 2313–2318.

Sterzer, P., & Rees, G. (2008). A neural basis for percept stabilization in binocular rivalry. *Journal of Cognitive Neuroscience*, *20*(3), 389–399.

Stettler, D. D., Das, A., Bennett, J., & Gilbert, C. D. (2002). Lateral connectivity and contextual interactions in macaque primary visual cortex. *Neuron*, *36*(4), 739–750.

Supèr, H., & Roelfsema, P. R. (2005). Chronic multiunit recordings in behaving animals: Advantages and limitations. *Progress in Brain Research*, *147*, 263–282.

Tanabe, S., & Cumming, B. G. (2014). Delayed suppression shapes disparity selective responses in monkey V1. *Journal of Neurophysiology*, *111*(9), 1759–1769.

Tong, F., & Engel, S. A. (2001, May 10). Interocular rivalry revealed in the human cortical blind-spot representation. *Nature*, *411*(6834), 195–199.

Tong, F., Meng, M., & Blake, R. (2006). Neural bases of binocular rivalry. *Trends in Cognitive Sciences*, *10*(11), 502–511.

Tong, F., Nakayama, K., Vaughan, J. T., & Kanwisher, N. (1998). Binocular rivalry and visual awareness in human extrastriate cortex. *Neuron*, *21*(4), 753–759.

Vastola, E. F. (1960). Binocular inhibition in the lateral geniculate body. *Experimental Neurology*, *2*(3), 221–231.

Walker, G. A., Ohzawa, I., & Freeman, R. D. (1998). Binocular cross-orientation suppression in the cat's striate cortex. *Journal of Neurophysiology*, *79*(1), 227–239.

Wheatstone, C. (1838). Contributions to the physiology of vision. Part the first. On some remarkable, and hitherto unobserved, phenomena of binocular vision. *Philosophical Transactions of the Royal Society of London*, *128*, 371–394.

Wilke, M., Logothetis, N. K., & Leopold, D. A. (2003). Generalized flash suppression of salient visual targets. *Neuron*, *39*(6), 1043–1052.

Wilke, M., Logothetis, N. K., & Leopold, D. A. (2006). Local field potential reflects perceptual suppression in monkey visual cortex. *Proceedings of the National Academy of Sciences, USA*, *103*(46), 17507–17512.

Wilke, M., Mueller, K.-M., & Leopold, D. A. (2009). Neural activity in the visual thalamus reflects perceptual suppression. *Proceedings of the National Academy of Sciences, USA*, *106*(23), 9465–9470.

Wilson, M. E., & Cragg, B. G. (1967). Projections from the lateral geniculate nucleus in the cat and monkey. *Journal of Anatomy*, *101*(4), 677–692.

Wolfe, J. M. (1983). Afterimages, binocular rivalry, and the temporal properties of dominance and suppression. *Perception*, *12*(4), 439–445.

Wolfe, J. M. (1984). Reversing ocular dominance and suppression in a single flash. *Vision Research*, *24*(5), 471–478.

Wunderlich, K., Schneider, K. A., & Kastner, S. (2005). Neural correlates of binocular rivalry in the human lateral geniculate nucleus. *Nature Neuroscience*, *8*(11), 1595–1602.

Yang, Z., Heeger, D. J., Blake, R., & Seidemann, E. (2015). Long-range traveling waves of activity triggered by local dichoptic stimulation in V1 of behaving monkeys. *Journal of Neurophysiology*, *113*(1), 277–294.

Yoshioka, T., Blasdel, G. G., Levitt, J. B., & Lund, J. S. (1996). Relation between patterns of intrinsic lateral connectivity, ocular dominance, and cytochrome oxidase-reactive regions in macaque monkey striate cortex. *Cerebral Cortex*, *6*(2), 297–310.

Downloaded from abstracts.iovs.org on 04/20/2024